J|A|C|S
ARTICLES
Published on Web 09/21/2004

# Density Functional Calculations of the $^{13}C$ NMR Chemical Shifts in (9,0) Single-Walled Carbon Nanotubes

Eva Zurek[†] and Jochen Autschbach*[,‡]

*Contribution from the Max-Planck-Institut für Festkörperforschung, Heisenbergstrasse 1, 70569, Stuttgart, Germany, and Department of Chemistry, University at Buffalo, 312 Natural Sciences Complex, State University of New York, Buffalo, New York 14260-3000*

Received April 9, 2004; E-mail: jochena@buffalo.edu

***Abstract:*** The electronic structure and $^{13}C$ NMR chemical shift of (9,0) single-walled carbon nanotubes (SWNTs) are investigated theoretically. Shielding tensor components are also reported. Density functional calculations were carried out for $C_{30}$-capped and H-capped fragments which serve as model systems for the infinite (9,0) SWNT. Based on the vanishing HOMO−LUMO gap, H-capped nanotube fragments are predicted to exhibit "metallic" behavior. The $^{13}C$ chemical shift approaches a value of ≈133 ppm for the longest fragment studied here. The $C_{30}$-capped SWNT fragments of $D_{3d}/D_{3h}$ symmetry, on the other hand, are predicted to be small-gap semiconductors just like the infinite (9,0) SWNT. The differences in successive HOMO−LUMO gaps and HOMO and LUMO energies, as well as the $^{13}C$ NMR chemical shifts, converge slightly faster with the fragment's length than for the H-capped tubes. The difference between the H-capped and $C_{30}$-capped fragments is analyzed in some detail. The results indicate that (at least at lengths currently accessible to quantum chemical computations) the H-capped systems represent less suitable models for the (9,0) SWNT because of pronounced artifacts due to their finite length. From our calculations for the $C_{30}$-capped fragments, the chemical shift of a carbon atom in the (9,0) SWNT is predicted to be about 130 ppm. This value is in reasonably good agreement with experimental estimates for the $^{13}C$ chemical shift in SWNTs.

## 1. Introduction

The discovery of carbon nanotubes[1] has sparked intense research activity within the past decade. These novel materials have a wide range of potential applications ranging from the fields of nanoelectronics to nanoscale biotechnology. For example they may be used as molecular field-effect transistors,[2,3] electron field emitters,[2,4] artificial muscles,[2,5] or even in DNA sequencing.[6] The wide horizon of applications stems from the fact that carbon nanotubes may have a diverse range of weights, electronic structures, helicities, etc. Individual classes of tubes exhibit very different physical and chemical properties. From a molecular design perspective, it is important to understand the experimental conditions necessary to produce tubes with a given subset of properties, and considerable effort has been placed into determining the parameters affecting the molecular architecture of the tubes.[4,7−9] Recently, advances in the separation of metallic and semiconducting tubes,[10,11] as well as tubes with different diameters,[11] have been made.

One of the reasons why it is so difficult to control the properties of the synthesized tubes is that there is no standalone method available by which they may be fully characterized. The length and diameter of an individual tube may be determined by AFM, STM or TEM. If information about the bulk sample is sought then SEM, X-ray diffraction, optical absorption and Raman scattering may be used. Unfortunately, even a combination of the aforementioned techniques does not fully characterize a given sample.[2]

The large decrease in price-to-performance ratio of modern CPUs, along with the implementation of favorably scaling density functional algorithms has recently made it possible to perform quantum-chemical calculations on the electronic struc-

[†] Max-Planck-Institut für Festkörperforschung.
[‡] State University of New York at Buffalo.

(1) Iijima, S. *Nature* **1991**, *354*, 56−58.
(2) Minett, A.; Atkinson, K.; Roth, S. Carbon nanotubes. In *Handbook of porous solids*; Schüth, F., Sing, S. W., Weitkamp, J., Eds.; Wiley-VCH: Weinheim, 2002.
(3) Yao, Z.; Postma, H. W. C.; Balents, L.; Dekker, C. *Nature* **1999**, *402*, 273−276.
(4) Zhou, O.; Shimoda, H.; Gao, B.; Oh, S.; Fleming, L.; Yue, G. *Acc. Chem. Res.* **2002**, *35*, 1045−1053.
(5) Baughman, R. H.; Cui, C.; Zakhidov, A. A.; Iqbal, Z.; Barisci, J. N.; Spinks, G. M.; Wallace, G. G.; Mazzoldi, A.; De Rossi, D.; Rinzler, A. G.; Jaschinski, O.; Roth, S.; Kertesz, M. *Science* **1999**, *284*, 1340−1344.
(6) Gao, H.; Kong, Y.; Cui, D. *Nano Lett.* **2003**, *3*, 471−473.
(7) Yudasaka, M.; Komatsu, T.; Ichihashi, T.; Achiba, Y.; Iijima, S. *J. Phys. Chem. B* **1998**, *102*, 4892−4896.
(8) Zhang, M.; Yudasaka, M.; Iijima, S. *J. Phys. Chem. B* **2004**, *108*, 149−153.
(9) Bandow, S.; Asaka, S.; Saito, Y.; Rao, A. M.; Grigorian, L.; Richter, E.; Eklund, P. C. *Phys. Rev. Lett.* **1998**, *80*, 3779−3782.
(10) Krupke, R.; Hennrich, F.; v. Löhneysen, H.; Kappes, M. M. *Science* **2003**, *301*, 344−347.
(11) Zheng, M.; Jagota, A.; Strano, M. S.; Santos, A. P.; Barone, P.; Chou, S. G.; Diner, B. A.; Dresselhaus, M. S.; McLean, R. S.; Onoa, G. B.; Samsonidze, G. G.; Semke, E. D.; Usrey, M.; Walls, D. J. *Science* **2003**, *302*, 1545−1548.

10.1021/ja047941m CCC: $27.50 

ture of large single-walled nanotube (SWNT) fragments.[12−18] Most computational solid-state and quantum-chemical studies of SWNTs have so far focused on geometric and electronic structure as well as mechanical properties. It is important to study electric and magnetic response properties as well, since they are the observables of some of the most powerful and frequently applied spectroscopic methods used for characterizing molecules. Among those, NMR is of high practical importance. Previous theoretical work proposed that separation of metallic from semiconducting SWNTs may be possible using high resolution $^{13}$C NMR, based on a predicted 11 ppm difference in their chemical shifts.[19,20] However, from the computations it was also concluded that NMR could not resolve the structural properties of SWNTs.[19] Values for the chemical shifts with respect to a standard reference were not reported in ref 19 because of neglected terms in the calculated shielding tensors (which were argued to be the same for different nanotube structures). It was indicated that the dependence of the NMR spectra on tube diameter and helicity might be weak among members of the metallic and semiconducting classes, respectively. So far only a few groups have used NMR to study the properties of nanotubes. The main difficulties arise from the large magnetic inhomogeneity in the samples caused by residual catalyst from the growth process. Before purification and annealing, very broad lines with about 1500 ppm anisotropy are observed.[20,21] MAS spectra measurements have yielded isotropic shifts of 124 ppm,[22] 116 ppm,[23] and 126 ppm with sidebands ranging over 300 ppm.[20,21] The exact composition of the sample was not determined.

Here, we present "molecular" density functional calculations of the $^{13}$C NMR chemical shift in SWNTs. We also report the principal components of the shielding tensors and indicate their orientation. Eventually, it will be desirable to perform a systematic study on nanotubes with different diameters, helicities, and electronic properties, the results of which could aid experimental characterization of nanotube samples. However, first it is necessary to determine suitable theoretical methods and structural models which must be used in order to obtain meaningful results. We believe that the chemical shift for the (9,0) SWNT reported here might already be useful in order to confirm that the aforementioned experimental estimates for the chemical shifts are within the same range as first-principles theoretical predictions. Within this study we will in particular focus on the following two issues:

(1) Are short SWNT fragments capped with hydrogen atoms good models for the electronic and magnetic response properties of closed SWNTs which are capped with half of a $C_{60}$ fragment?

(2) How do the SWNT's electronic and magnetic properties depend on the size of the tube? In particular, do these properties converge with increasing tube length, indicating that calculations on finite sized tubes are able to give any insight into a system of infinite length?

## 2. Methodology, Computational Details

The computations were performed with the Amsterdam Density Functional (ADF) code.[24,25] In all calculations we have applied the revised Perdew−Burke−Ernzerhof (revPBE) nonhybrid density functional.[26−29] Full geometry optimizations of all SWNT fragments as well as $C_{60}$ and the NMR reference tetramethylsilane (TMS) were carried out employing a valence triple-ζ Slater type basis set with polarization functions for all atoms (TZP) from the ADF basis set library. The 1s shells of the carbon atoms were kept frozen for the geometry optimizations. NMR chemical shift calculations were carried out with the all-electron TZP basis set (which is of double-ζ quality for the carbon 1s shells) and the revPBE functional, employing the nonrelativistic GIAO (gauge-including atomic orbitals) methodology developed by Schreckenbach and Ziegler[30−33] as implemented in the "NMR" program of the ADF package. NMR chemical shifts are reported with respect to TMS whose shielding was calculated as being 185.10 ppm at this level. Because of the computational expense for the two largest molecules studied here (the 204 and 222 carbon atom fragments), not all possible chemical shifts from symmetry inequivalent atoms could be calculated. However, a representative subset which includes a number of atoms from the end to the middle of each tube fragment has been considered. We believe that this is sufficient in order to allow conclusions about the trends which are of interest here. For the other systems, the chemical shifts for all symmetry inequivalent carbons were calculated. To assess the accuracy of our results, calculations with various basis sets and another functional were performed on a subset of systems studied here. The results of these calculations are discussed in section 3.

Due to the fact that ADF does not support $D_{9h}/D_{9d}$ symmetry, calculations on the hydrogen capped tubes were carried out in the $D_{3h}/D_{3d}$ subgroups. This also facilitates comparisons with the $C_{30}$ capped SWNT fragments. For the $C_{30}$-capped tubes, $D_{3h}/D_{3d}$ symmetry was employed with the exception of one $D_3$ tube which was considered for comparison. For both the smallest hydrogen and $C_{30}$-capped SWNT fragments, single-point calculations without symmetry constraints were also performed. Within the numerical accuracy of the computations, the results showed identical orbital occupancies, orbital energies, and total energies to the calculations performed using symmetry constraints. However, the calculations without symmetry needed a larger number of SCF cycles in order to reach charge density convergence.

(12) Cioslowski, J.; Rao, N.; Moncrieff, D. *J. Am. Chem. Soc.* **2002**, *124*, 8485−8489.
(13) Zhou, Z.; Steigerwald, M.; Hybertsen, M.; Brus, L.; Friesner, R. A. *J. Am. Chem. Soc.* **2004**, *126*, 3597−3607.
(14) Yumura, T.; Hirahara, K.; Bandow, S.; Yoshizawa, K.; Iijima, S. *Chem. Phys. Lett.* **2004**, *386*, 38−43.
(15) Nomura, Y.; Fujita, H.; Narita, S.; Shibuya, T. *Chem. Phys. Lett.* **2003**, *375*, 72−75.
(16) Cioslowski, J.; Rao, N.; Pernal, K.; Moncrieff, D. *J. Chem. Phys.* **2003**, *118*, 4456−4462.
(17) Reiher, M.; Neugebauer, J. *J. Chem. Phys.* **2003**, *118*, 1634−1641.
(18) Rochefort, A.; Salahub, D. R.; Avouris, P. *J. Phys. Chem. B.* **1999**, *103*, 641−646.
(19) Latil, S.; Henrard, L.; Goze Bac, C.; Bernier, P.; Rubio, A. *Phys. Rev. Lett.* **2001**, *86*, 3160−3163.
(20) Goze-Bac, C.; Latil, S.; Lauginie, P.; Jourdain, V.; Conard, J.; Duclaux, L.; Rubio, A.; Bernier, P. *Carbon* **2002**, *40*, 1825−1842.
(21) Goze Bac, C.; Latil, S.; Vaccarini, L.; Bernier, P.; Gaveau, P.; Tahir, S.; Micholet, V.; Aznar, R. *Phys. Rev. B* **2001**, *63*, 100302-1−100302-4.
(22) Tang, X.-P.; Kleinhammes, A.; Shimoda, H.; Fleming, L.; Bennoune, K. Y.; Shina, S.; Bower, C.; Zhou, O.; Wu, Y. *Science* **2000**, *288*, 492−494.
(23) Hayashi, S.; Hoshi, F.; Ishikura, T.; Yumura, M.; Ohshima, S. *Carbon* **2003**, *41*, 3047−3056.
(24) Baerends, E. J. et al. *Amsterdam Density Functional*; Theoretical Chemistry, Vrije Universiteit: Amsterdam, URL http://www.scm.com.
(25) te Velde, G.; Bickelhaupt, F. M.; Baerends, E. J.; van Gisbergen, S. J. A.; Fonseca Guerra, C.; Snijders, J. G.; Ziegler, T. *J. Comput. Chem.* **2001**, *22*, 931−967.
(26) Perdew, J. P.; Burke, K.; Ernzerhof, M. *Phys. Rev. Lett.* **1996**, *77*, 3865−3868.
(27) Zhang, Y.; Yang, W. *Phys. Rev. Lett.* **1998**, *80*, 890.
(28) Perdew, J. P.; Burke, K.; Ernzerhof, M. *Phys. Rev. Lett.* **1998**, *80*, 891.
(29) Hammer, B.; Hansen, L. B.; Norskov, J. K. *Phys. Rev. B* **1999**, *59*, 7413−7421.
(30) Schreckenbach, G.; Ziegler, T. *J. Phys. Chem.* **1995**, *99*, 606−611.
(31) Schreckenbach, G.; Ziegler, T. *Int. J. Quantum Chem.* **1996**, *60*, 753−766.
(32) Schreckenbach, G.; Dickson, R. M.; Ruiz-Morales, Y.; Ziegler, T. The calculation of NMR parameters by density-functional theory. In *Chemical Applications of Density-Functional Theory*, Vol. 629; Laird, B. B., Ross, R. B., Ziegler, T., Eds.; American Chemical Society: Washington, DC, 1996.
(33) Schreckenbach, G.; Ziegler, T. *Theor. Chem. Acc.* **1998**, *99*, 71−82.

The authors of ref 12 have applied a correction to the HOMO−LUMO energy difference when reporting estimated band gaps for the (5,5) and the (9,0) SWNTs. The correction was obtained from considering Koopmans' theorem for the $C_{60}$ fullerene, under the assumption that errors of similar magnitudes may be present for the $C_{30}$-capped SWNTs. The average of available experimental values for the IP of $C_{60}$ is 7.56 eV,[34−37] the average of experimentally determined EAs is 2.68 eV.[38,39] Our calculated orbital energies of 6.05 eV (HOMO) and 4.40 eV (LUMO) are of similar magnitude as the 6.40 and 3.66 eV, respectively, from the DFT (B3LYP hybrid functional) calculations in ref 12. If calculated HOMO−LUMO gaps are to be identified with IP−EA and with the band gap of the SWNT it is seen that the calculated value for $C_{60}$ is too large. Correction terms of −1.51 and 1.72 eV might therefore be added to the HOMO and LUMO energies, as was done previously in ref 12. However, it was noted there that such a correction leads to a clear overestimation of the band gap. For DFT calculations, the HOMO−LUMO gap serves as a zeroth-order estimate of the lowest excitation energy of the system[40] rather than IP−EA which could explain why the application of the correction term leads to the aforementioned overestimation. For comparison with the results of ref 12, in the following both the corrected and uncorrected values are given for the $C_{30}$-capped SWNTs.

A subset of the graphics were prepared using the XCRYSDEN program.[41] The orbital isosurface plots were created with the program MOLEKEL.[42] Figure 12 was prepared using MATHEMATICA.

## 3. Results and Discussion

**3.1. Electronic Structure of (9,0) SWNTs.** A SWNT can be constructed from the rolling of a graphene sheet. It can be uniquely classified by a vector, or more conveniently a pair of numbers ($n_1$, $n_2$), connecting the two points which meet upon rolling. This results in three classes of tubes: armchair, zigzag, and helical (chiral) characterized by ($n$, $n$), ($n$, 0), ($n_1$, $n_2$), respectively. Early tight-binding calculations on a graphene sheet model showed that SWNTs should exhibit metallic characteristics if and only if

$$n_1 - n_2 = 3q \tag{1}$$

where $q$ is an integer.[43,44] However, models which considered hybridization between $\pi$-orbitals perpendicular to the normal of the tube and $sp^2$-$\sigma$ orbitals showed that tubes satisfying eq 1, but for which $n_1 \neq n_2$, were found to be narrow-gap semiconductors.[43−45] The band gap was predicted to decrease as the diameter of the tube increased, due to the reduction of hybridization.[44,43] Tubes for which $n_1 = n_2$ were found to be metallic due to symmetry.[43−46] Hybridization between $\sigma^*$ and $\pi^*$ orbitals has also been shown to have an effect on the electronic structure of small-radius nanotubes.[47] Low-temperature STM investigations revealed band gaps of $0.080 \pm 0.005$, $0.042 \pm 0.004$, and $0.029 \pm 0.004$ eV for the (9,0), (12,0), and (15,0) SWNTs, respectively.[48] In a recent paper studying the electronic structure of (9,0) and (5,5) SWNTs capped by half of a fullerene, Cioslowski and co-workers showed that the former have a finite HOMO−LUMO gap which appears to converge well with increasing tube length.[12] These results have been confirmed by another group.[14]

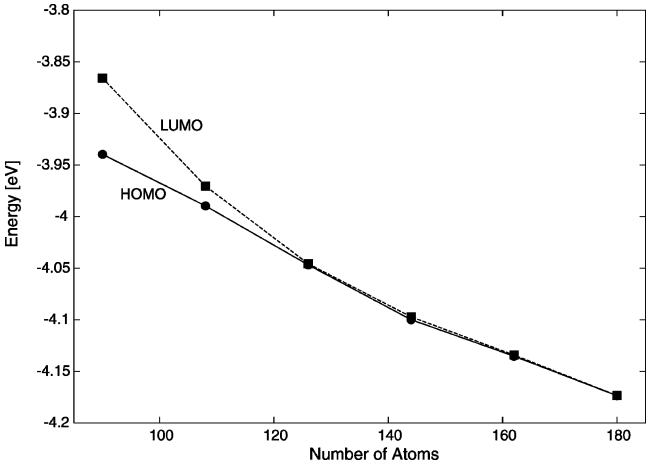


***Figure 1.*** HOMO−LUMO gaps of hydrogen capped $D_{9h}$/$D_{9d}$ (9,0) SWNTs. The total number of atoms in the tube is given along the abscissa.

Due to the absence of periodic boundary conditions in molecular calculations, it is necessary to saturate the carbon dangling bonds in nanotube fragments. Often, hydrogen is assumed to be a good choice.[13,17,18,49] Each ring segment of the (9,0) tube consists of 18 atoms, and therefore such hydrogen capped tube fragments consisting of $N$ segments contain $18N$ carbon atoms. This results in fragments with $D_{9h}$ or $D_{9d}$ symmetry for even and odd $N$, respectively. The HOMO−LUMO gaps and difference between HOMO−LUMO gaps for successively larger fragments of the hydrogen capped tubes are given in Figures 1 and 2. The number of atoms given along the abscissa also includes the capping hydrogens, thus $N =$ (number of atoms)/18 − 1. The symmetry of the tubes changes with increasing $N$, and we have indicated in Figure 2 the differences for each symmetry separately. They are either given by

$$\Delta\Delta E_{D_{9h}} = \Delta E(D_{9h}) - \Delta E \quad (\text{next shorter fragment of } D_{9d} \text{ symmetry}) \tag{2}$$

or by

$$\Delta\Delta E_{D_{9d}} = \Delta E(D_{9d}) - \Delta E \quad (\text{next shorter fragment of } D_{9h} \text{ symmetry}) \tag{3}$$

Clearly, a hydrogen capped (9,0) tube is predicted to be metallic

(34) Hertel, I. V.; Steger, H.; de Vries, J.; Weisser, B.; Menzel, C.; Kamke, B.; Kamke, W. *Phys. Rev. Lett.* **1992**, *68*, 784−787.
(35) Yoo, R. K.; Ruscic, B.; Berkowitz, J. *J. Chem. Phys.* **1992**, *96*, 911−918.
(36) de Vries, J.; Steger, H.; Kamke, B.; Menzel, C.; Weisser, B.; Kamke, W.; Hertel, I. V. *Chem. Phys. Lett.* **1992**, *188*, 159−162.
(37) Steger, H.; Holzapfel, J.; Hielscher, A.; Kamke, W.; Hertel, I. V. *Chem. Phys. Lett.* **1995**, *234*, 455−459.
(38) Brink, C.; Andersen, L. H.; Hvelplund, P.; Mathur, D.; Voldstad, J. D. *Chem. Phys. Lett.* **1995**, *233*, 52−56.
(39) Wang, X. B.; Ding, C.-F.; Wang, L.-S. *J. Chem. Phys.* **1999**, *110*, 8217−8220.
(40) Casida, M. E. Time-dependent density functional response theory for molecules. In *Recent advances in density functional methods*, Vol. 1; Chong, D. P., Ed.; World Scientific: Singapore, 1995.
(41) Kokalj, A. *J. Mol. Graphics Modelling* **1999**, *17*, 176−179 Code available from http://www.xcrysden.org/.
(42) Flükiger, P.; Lüthi, H.; Portmann, S.; Weber, J. *Molekel 4.0*; Swiss Center for Scientific Computing: Manno, Switzerland, 2000.
(43) White, C. T.; Robertson, D. H.; Mintmire, J. W. *Phys. Rev. B* **1993**, *47*, 5485−5488.
(44) Saito, R.; Fujita, M.; Dresselhaus, G.; Dresselhaus, M. S. *Phys. Rev. B* **1992**, *46*, 1804−1811.
(45) Hamada, N.; Sawada, S.; Oshiyama, A. *Phys. Rev. Lett.* **1992**, *68*, 1579−1581.
(46) Mintmire, J. W.; Dunlap, B. I.; White, C. T. *Phys. Rev. Lett.* **1992**, *68*, 631−634.
(47) Blase, X.; Benedict, L. X.; Shirley, E. L.; Louie, S. G. *Phys. Rev. Lett.* **1994**, *72*, 1878−1881.
(48) Ouyang, M.; Huang, J.-L.; Cheung, C. L.; Lieber, C. M. *Science* **2001**, *292*, 702−705.
(49) Bulusheva, L. G.; Okotrub, A. V.; Romanov, D. A.; Tomanek, D. *J. Phys. Chem. A* **1998**, *102*, 975−981.

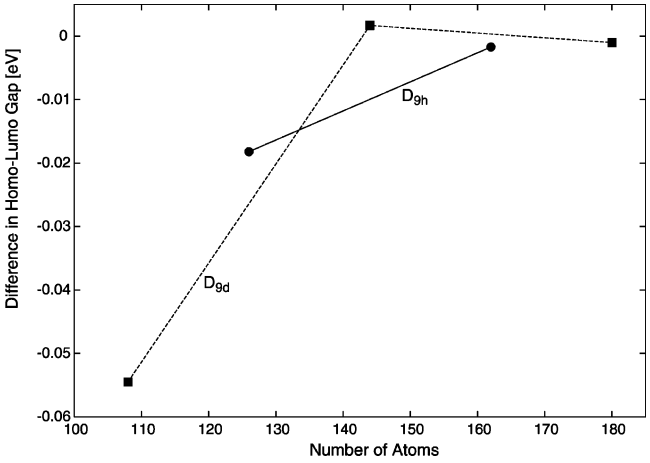


***Figure 2.*** Difference between successive HOMO−LUMO gaps in hydrogen capped $D_{9h}/D_{9d}$ (9,0) SWNTs. The lines do not represent a fit to the data but were added to guide the eye. See also eqs 2 and 3. The total number of atoms in the tube is given along the abscissa.

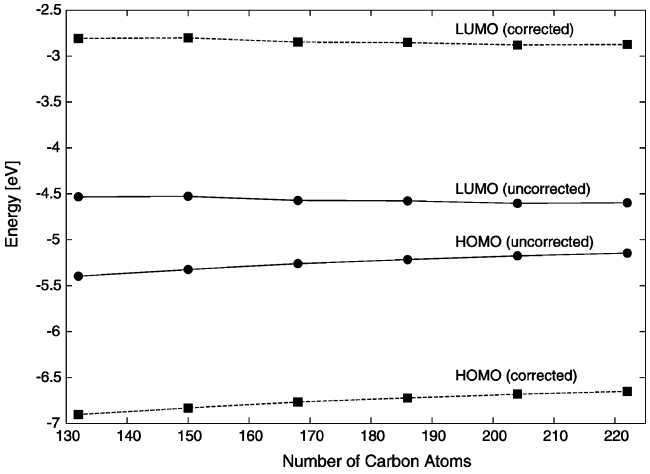


***Figure 3.*** HOMO−LUMO gaps of $C_{30}$-capped $D_{3h}/D_{3d}$ (9,0) SWNT fragments. The total number of atoms in the tube is given along the abscissa.

starting with $N \approx 6$. This result appears to be well converged with respect to the length of the SWNT studied here. The HOMOs and LUMOs for the H-capped SWNT fragments are found to be of $E$ symmetry and therefore doubly degenerate. This agrees with previous calculations on hydrogen capped ($n$, 0) tubes showing that $n = 6, 8, 10$ afforded nondegenerate and $n = 7, 9, 11$ yielded doubly degenerate HOMOs and LUMOs.[49]

It is also possible to cap a (9,0) zigzag SWNT with half of a $C_{60}$ fullerene, yielding two sets of $C_{60 + 18j}$ tubes.[12,50] In the first set, even/odd $j$ gives $D_{3d}/D_{3h}$ symmetry. Rotation of one of the $C_{30}$ caps by 40° produces members from the second set which possess $D_3$ symmetry. It has previously been shown that the members of the former are energetically more stable and have larger HOMO−LUMO gaps than those of the latter,[12] and therefore the focus of this study is on SWNTs possessing $D_{3d}/D_{3h}$ symmetry. The HOMO−LUMO gaps and difference between HOMO−LUMO gaps for successively larger $C_{30}$-capped tubes are displayed in Figures 3 and 4. The uncorrected HOMO−LUMO gaps are approximately half the size which were previously calculated using the B3LYP functional.[12,14] The corrected ones are approximately 1.1 times larger than those

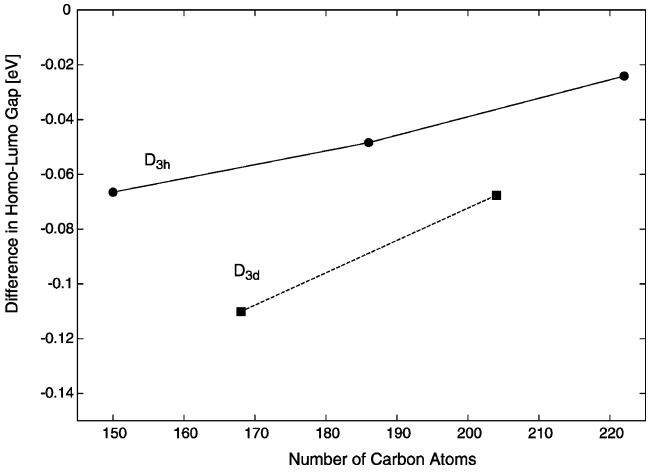


***Figure 4.*** Difference between successive HOMO−LUMO gaps in $C_{30}$-capped $D_{3h}/D_{3d}$ (9,0) SWNT fragments. The total number of atoms in the tube is given along the abscissa. The lines to not represent a fit to the data but were added to guide the eye. See also eqs 2 and 3, but with $D_{9h}/D_{9d}$ replaced by $D_{3h}/D_{3d}$.

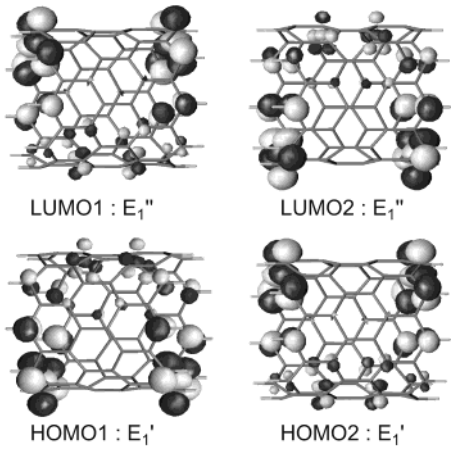


***Figure 5.*** Two HOMO and two LUMO orbitals for the $D_{9h}$, 90 atom, hydrogen capped SWNT. Isosurface for ±0.03 au.

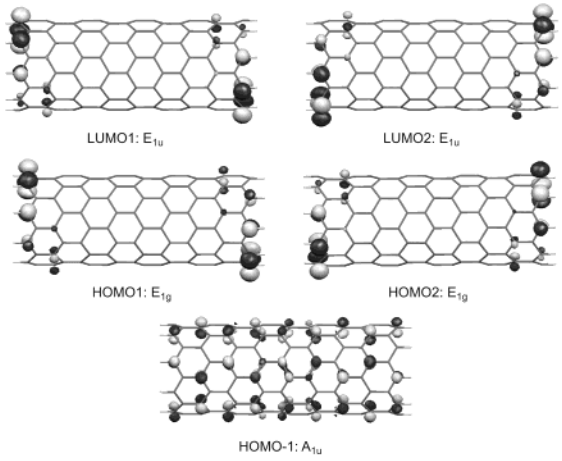


***Figure 6.*** Two HOMO and two LUMO orbitals for the $D_{9d}$, 180 atom, hydrogen capped SWNT. Also shown is the (HOMO-1) $A_{1u}$ orbital. Isosurface for ±0.03 au for the HOMO and LUMO and ±0.025 au for the (HOMO-1).

reported in previous work,[12] due to the fact that the computational methodology employed here produced a smaller HOMO−LUMO gap for $C_{60}$ and therefore a larger correction was added. These differences are not surprising, since it is known that, for

(50) Dresselhaus, M. S.; Dresselhaus, G.; Saito, R. *Phys. Rev. B* **1992**, *45*, 6234−6242.

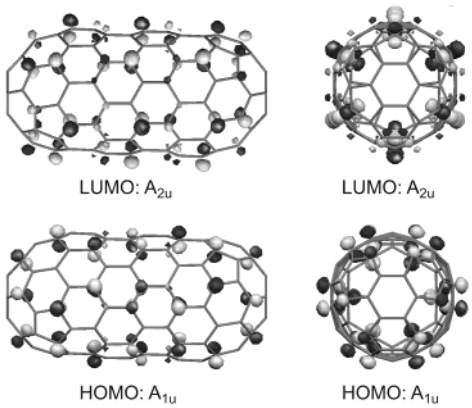


***Figure 7.*** HOMO and LUMO orbitals for the $D_{3d}$, 132 atom, $C_{30}$ capped SWNT. Isosurface for $\pm 0.03$ au.

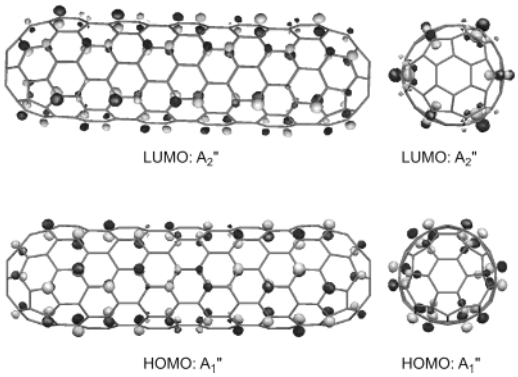


***Figure 8.*** HOMO and LUMO orbitals for the $D_{3h}$, 222 atom, $C_{30}$ capped SWNT. Isosurface for $\pm 0.025$ au.

***Table 1.*** Dependence of the $^{13}C$ Nuclear Shielding and Chemical Shift in $C_{60}$ on Basis Set and Density Functional[a]

| basis | functional | shielding | TMS[b] | shift |
|---|---|---|---|---|
| DZ | revPBE | 57.654 | 203.96 | 146.31 |
| DZP | revPBE | 53.506 | 192.07 | 138.56 |
| TZP | revPBE | 39.265 | 185.10 | 145.84 |
| TZ2P | revPBE | 38.723 | 185.63 | 146.91 |
| DZ | VWN | 51.706 | 202.32 | 150.61 |
| DZP | VWN | 46.950 | 190.57 | 143.62 |
| TZP | VWN | 29.835 | 182.71 | 152.88 |
| TZ2P | VWN | 29.144 | 183.28 | 154.14 |

[a] Experimental chemical shift: 142.68 ppm. [b] Calculated shielding constant for TMS.

***Table 2.*** Dependence of the Calculated $^{13}C$ Chemical Shift in the 90-Atom H-Capped (9,0) SWNT Fragment on the Basis Set (revPBE Functional)

| nucleus[a] | basis | shift[b] |
|---|---|---|
| 1 | DZ | 128.51 |
| | DZP | 121.20 |
| | TZP | 128.69 |
| | TZ2P | 130.22 |
| 2 | DZ | 143.69 |
| | DZP | 137.64 |
| | TZP | 147.14 |
| | TZ2P | 148.35 |
| 3 | DZ | 136.37 |
| | DZP | 129.11 |
| | TZP | 136.87 |
| | TZ2P | 138.16 |
| 4 | DZ | 136.20 |
| | DZP | 129.60 |
| | TZP | 137.99 |
| | TZ2P | 139.28 |

[a] The numbers refer to the numbering scheme chosen in Figure 9. [b] With respect to TMS. The calculated $^{13}C$ shielding constants for TMS are listed in Table 1.

***Table 3.*** Dependence of the Calculated $^{13}C$ Chemical Shift in the 108-Atom H-Capped (9,0) SWNT Fragment on the Basis Set (revPBE Functional)

| nucleus[a] | basis | shift[b] |
|---|---|---|
| 1 | DZ | 127.40 |
| | DZP | 119.84 |
| | TZP | 127.12 |
| | TZ2P | 128.66 |
| 2 | DZ | 134.01 |
| | DZP | 128.00 |
| | TZP | 136.38 |
| | TZ2P | 137.61 |
| 3 | DZ | 133.90 |
| | DZP | 127.62 |
| | TZP | 135.50 |
| | TZ2P | 136.83 |
| 4 | DZ | 133.37 |
| | DZP | 126.35 |
| | TZP | 133.87 |
| | TZ2P | 135.10 |
| 5 | DZ | 141.32 |
| | DZP | 135.29 |
| | TZP | 144.34 |
| | TZ2P | 145.61 |

[a] The numbers refer to the numbering scheme chosen in Figure 9. [b] With respect to TMS. The calculated $^{13}C$ shielding constants for TMS are listed in Table 1.

many compounds containing C, H, N, O, the B3LYP hybrid functional applied in ref 12 results in HOMO−LUMO gaps which are larger than those calculated with nonhybrid density functionals such as the one applied here (PBE). Regardless of the addition of a correction term, the results are seen to converge to a finite HOMO−LUMO gap. This can be seen most clearly in Figure 4 which shows that the difference between successive HOMO−LUMO gaps, $\Delta\Delta E$, approaches zero with increasing length of the tube. The symmetry of the tubes changes with increasing $j$ which leads to an oscillatory behavior of the HOMO−LUMO gap when comparing SWNT fragments of different symmetry. To avoid this we have indicated in Figure 4 the differences for each symmetry separately. These $\Delta\Delta E$ values converge rapidly to zero without displaying further oscillatory behavior. A rough estimate of the lengths of the tubes for which $\Delta\Delta E_{D_{3h}}$ and $\Delta\Delta E_{D_{3d}}$ approach zero was obtained through a linear fit of the two sets of $\Delta\Delta E$'s and extrapolation to $\Delta\Delta E = 0$. The first series is predicted to converge at ~276 carbon atoms, and the second, at ~312. It must also be noted that the HOMOs and LUMOs of these species are spatially nondegenerate, unlike the frontier orbitals for the H-capped SWNT fragments.

The results indicate that hydrogen capped (9,0) SWNT fragments are metallic, whereas ones capped with a $C_{30}$ hemisphere are small-gap semiconductors. Moreover, the HOMOs and LUMOs of the former are doubly degenerate, whereas those of the latter are nondegenerate. These findings indicate that in this case *a hydrogen capped tube is not a good model for a $C_{30}$-capped tube*. It is also not a good model for an infinite tube which is predicted to be a small-gap semiconductor by band structure calculations[43−45,47] and experimental measurements.[48]

For the $D_{3d}/D_{3h}$ $C_{30}$-capped tubes, the HOMOs are of $A_{1u}/A_1''$ symmetry and the LUMOs are of $A_{2u}/A_2''$ symmetry. For the $D_{9h}$ hydrogen capped tubes which were calculated in $D_{3h}$ symmetry, these frontier orbitals have either $E_1'$ or $E_1''$

***Table 4.*** Dependence of the Calculated $^{13}C$ Chemical Shift in the 132-Atom $C_{30}$-Capped (9,0) SWNT Fragment on the Basis Set (revPBE functional)

| nucleus[a] | basis | shift[b] | nucleus[a] | basis | shift[b] |
|---|---|---|---|---|---|
| 1 | DZ | 152.18 | 8 | DZ | 147.94 |
| | DZP | 146.16 | | DZP | 140.42 |
| | TZP | 153.77 | | TZP | 148.20 |
| 2 | DZ | 151.26 | 9 | DZ | 141.06 |
| | DZP | 144.66 | | DZP | 134.94 |
| | TZP | 152.67 | | TZP | 142.52 |
| 3 | DZ | 134.87 | 10 | DZ | 133.05 |
| | DZP | 128.40 | | DZP | 126.46 |
| | TZP | 135.62 | | TZP | 134.31 |
| 4 | DZ | 133.85 | 11 | DZ | 132.05 |
| | DZP | 126.75 | | DZP | 125.15 |
| | TZP | 134.57 | | TZP | 131.99 |
| 5 | DZ | 129.14 | 12 | DZ | 131.62 |
| | DZP | 122.62 | | DZP | 124.98 |
| | TZP | 130.19 | | TZP | 132.48 |
| 6 | DZ | 132.49 | 13 | DZ | 139.71 |
| | DZP | 125.63 | | DZP | 133.51 |
| | TZP | 133.84 | | TZP | 140.68 |
| 7 | DZ | 145.03 | 14 | DZ | 147.09 |
| | DZP | 137.40 | | DZP | 140.05 |
| | TZP | 145.22 | | TZP | 147.79 |

[a] The numbers refer to the numbering scheme chosen in Figure 10. [b] With respect to TMS. The calculated $^{13}C$ shielding constants for TMS are listed in Table 1.

***Table 5.*** Dependence of the Calculated $^{13}C$ Chemical Shift in the 150-Atom $C_{30}$-Capped (9,0) SWNT Fragment on the Basis Set (revPBE Functional)

| nucleus[a] | basis | shift[b] | nucleus[a] | basis | shift[b] |
|---|---|---|---|---|---|
| 1 | DZ | 152.64 | 9 | DZ | 133.15 |
| | DZP | 146.85 | | DZP | 126.47 |
| | TZP | 154.65 | | TZP | 134.12 |
| 2 | DZ | 151.45 | 10 | DZ | 148.57 |
| | DZP | 144.86 | | DZP | 141.23 |
| | TZP | 152.93 | | TZP | 149.02 |
| 3 | DZ | 135.35 | 11 | DZ | 145.29 |
| | DZP | 128.86 | | DZP | 137.88 |
| | TZP | 135.96 | | TZP | 145.65 |
| 4 | DZ | 134.18 | 12 | DZ | 132.31 |
| | DZP | 127.04 | | DZP | 125.50 |
| | TZP | 134.76 | | TZP | 133.21 |
| 5 | DZ | 129.15 | 13 | DZ | 129.59 |
| | DZP | 122.43 | | DZP | 123.16 |
| | TZP | 130.02 | | TZP | 130.76 |
| 6 | DZ | 146.63 | 14 | DZ | 140.74 |
| | DZP | 139.59 | | DZP | 134.56 |
| | TZP | 147.28 | | TZP | 141.92 |
| 7 | DZ | 139.72 | 15 | DZ | 134.38 |
| | DZP | 133.27 | | DZP | 127.96 |
| | TZP | 140.54 | | TZP | 135.39 |
| 8 | DZ | 131.89 | 16 | DZ | 129.32 |
| | DZP | 125.40 | | DZP | 122.61 |
| | TZP | 133.10 | | TZP | 129.87 |

[a] The numbers refer to the numbering scheme chosen in Figure 10. [b] With respect to TMS. The calculated $^{13}C$ shielding constants for TMS are listed in Table 1.

symmetry. For the $D_{9d}$ hydrogen capped tubes which were calculated in $D_{3d}$ symmetry, they are of either $E_{1u}$ or $E_{1g}$ symmetry. Due to the fact that these orbitals are so close in energy, the order of their population is sometimes reversed. Band structure calculations which did not take into account $\sigma$-$\pi$ hybridization and hence predicted metallic behavior for the zigzag fibers showed that the highest occupied and lowest unoccupied bands were 2-fold degenerate of $E$ symmetry, touching the Fermi level at the $\Gamma$ point.[44]

In Figures 5−8, the HOMOs and LUMOs for the smallest and largest tubes with each capping are presented in form of isosurface plots. All of these frontier orbitals have carbon p-$\pi$ character; however, in the case of the hydrogen capped SWNTs, they are localized at each end of the tube, whereas, for the $C_{30}$-capped SWNTs, they are delocalized over the whole fragment. At the same time, it can be seen from Figures 6 and 8 that the HOMO-1 of $A_{1u}$ symmetry of the H-capped fragment resembles the HOMO of the $C_{30}$-capped 222 atom fragment. Since the HOMOs and LUMOs of the H-capped systems are localized at the ends of the fragments, it is obvious that they do not represent an occupied orbital of an infinite system. As the length of the fragment increases, these orbitals do not yield a contribution to the electron density along the tube (except at the ends) and must therefore be regarded as artifacts due to treating the finite-sized systems. On the other hand, the HOMOs and LUMOs of the $C_{30}$-capped systems indeed seem to yield a good representation of the band structure of the infinite systems at the $\Gamma$ point. We expect that for very long H-capped fragments the HOMO-1 and LUMO+1 shape and energy become similar to the HOMOs and LUMOs of the corresponding $C_{30}$-capped fragments. It

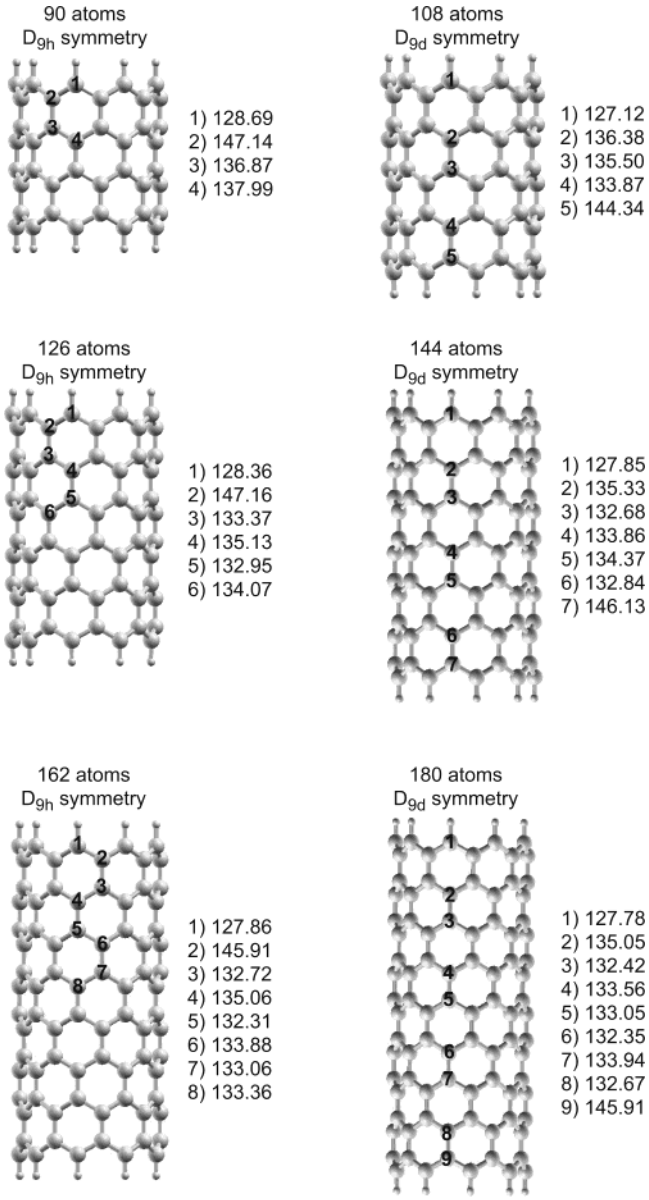


***Figure 9.*** $^{13}C$ NMR chemical shifts of hydrogen capped $D_{9h}/D_{9d}$ (9,0) SWNTs, with respect to TMS. revPBE functional, TZP basis.

132 atoms
$D_{3d}$ symmetry

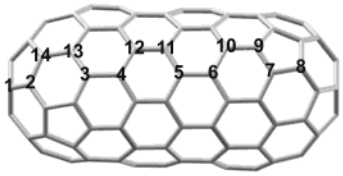


| | | |
|---|---|---|
| 1) 153.77 | 6) 133.84 | 11) 131.99 |
| 2) 152.67 | 7) 145.22 | 12) 132.48 |
| 3) 135.62 | 8) 148.20 | 13) 140.68 |
| 4) 134.57 | 9) 142.52 | 14) 147.79 |
| 5) 130.19 | 10) 134.31 | |

150 atoms
$D_{3h}$ symmetry

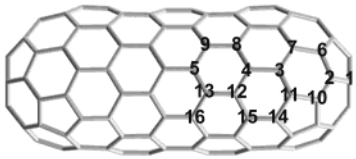


| | | |
|---|---|---|
| 1) 154.65 | 7) 140.54 | 13) 130.76 |
| 2) 152.93 | 8) 133.10 | 14) 141.92 |
| 3) 135.96 | 9) 134.12 | 15) 135.39 |
| 4) 134.76 | 10) 149.02 | 16) 129.87 |
| 5) 130.02 | 11) 145.65 | |
| 6) 147.28 | 12) 133.21 | |

168 atoms
$D_{3d}$ symmetry

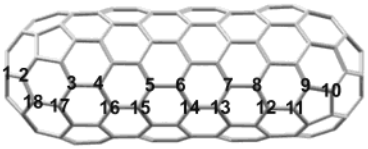


| | | |
|---|---|---|
| 1) 155.31 | 7) 129.49 | 13) 128.85 |
| 2) 153.07 | 8) 131.33 | 14) 131.77 |
| 3) 136.26 | 9) 144.93 | 15) 136.07 |
| 4) 133.26 | 10) 149.20 | 16) 129.90 |
| 5) 131.22 | 11) 140.30 | 17) 141.59 |
| 6) 127.43 | 12) 136.22 | 18) 146.96 |

186 atoms
$D_{3h}$ symmetry

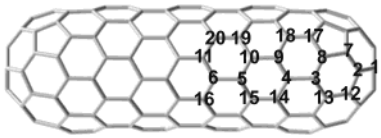


| | | |
|---|---|---|
| 1) 155.96 | 8) 145.10 | 15) 135.86 |
| 2) 152.89 | 9) 133.09 | 16) 131.23 |
| 3) 136.35 | 10) 130.79 | 17) 139.76 |
| 4) 133.83 | 11) 129.89 | 18) 136.86 |
| 5) 129.61 | 12) 146.04 | 19) 127.60 |
| 6) 130.74 | 13) 141.19 | 20) 132.89 |
| 7) 149.63 | 14) 131.33 | |

204 atoms
$D_{3d}$ symmetry

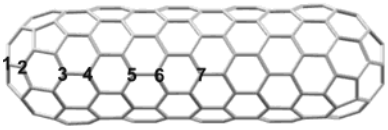


| | | |
|---|---|---|
| 1) 156.14 | 4) 133.29 | 7) 129.20 |
| 2) 153.25 | 5) 129.64 | |
| 3) 136.13 | 6) 130.61 | |

222 atoms
$D_{3h}$ symmetry

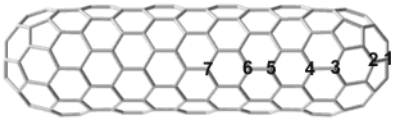


| | | |
|---|---|---|
| 1) 156.25 | 4) 133.32 | 7) 129.86 |
| 2) 152.96 | 5) 129.74 | |
| 3) 136.78 | 6) 129.81 | |

***Figure 10.*** $^{13}C$ NMR chemical shifts of $C_{30}$-capped $D_{3h}/D_{3d}$ (9,0) SWNTs, with respect to TMS. revPBE functional, TZP basis.

appears that the H-capped fragments are not well converged in this respect. Both the HOMO-1s and HOMOs of the H-capped fragments have contributions at the tube ends which means that there should be comparatively large Coulomb interactions present between these orbitals which are slowly vanishing with increasing length.

**3.2. NMR Chemical Shifts of (9,0) SWNTs.** Our calculated value of the $^{13}C$ NMR chemical shift in $C_{60}$ is 145.84 ppm. It compares reasonably well with the experimental value of 142.68 ppm.[51] To assess the dependence of our results on basis set and approximate density functional, we have carried out additional calculations for $C_{60}$ and some of the smaller nanotube fragments. The data for $C_{60}$ are collected in Table 1.

132 atoms
$D_3$ symmetry

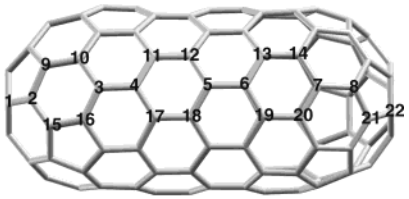


| | | |
|---|---|---|
| 1) 157.22 | 9) 156.33 | 16) 143.34 |
| 2) 148.71 | 10) 145.96 | 17) 127.74 |
| 3) 135.40 | 11) 135.48 | 18) 136.54 |
| 4) 129.26 | 12) 124.12 | 19) 131.69 |
| 5) 130.83 | 13) 138.45 | 20) 137.92 |
| 6) 133.43 | 14) 132.36 | 21) 154.62 |
| 7) 140.09 | 15) 143.60 | 22) 159.88 |
| 8) 148.27 | | |

***Figure 11.*** $^{13}C$ NMR chemical shifts of a 132 atom, $C_{30}$-capped $D_3$ (9,0) SWNT, with respect to TMS.

(51) Taylor, R.; Hare, J. P.; Abdul-Sada, A. K.; Kroto, H. W. *J. Chem. Soc., Chem. Commun.* **1990**, *20*, 1423−1424.

***Table 6.*** Principal Components of the Shielding Tensors $\sigma$ for $C_{60}$ and the H-Capped (9,0) SWNT Fragments, Calculated at the TZP/revPBE Level

| system | no.[a] | $\sigma_{11}$ | $\sigma_{22}$ | $\sigma_{33}$ | system | no.[a] | $\sigma_{11}$ | $\sigma_{22}$ | $\sigma_{33}$ |
|---|---|---|---|---|---|---|---|---|---|
| $C_{60}$ | | −26.037 | −21.053 | 164.885 | H-cap | 1 | −13.690 | 46.971 | 144.448 |
| | | | | | 162 atoms | 2 | −31.942 | −15.694 | 163.420 |
| H-cap | 1 | −24.405 | 50.914 | 142.713 | | 3 | −14.133 | −3.864 | 174.103 |
| 90 atoms | 2 | −40.630 | −13.914 | 168.437 | | 4 | −15.511 | −9.376 | 172.281 |
| | 3 | −27.934 | −2.098 | 174.733 | | 5 | −11.593 | −7.296 | 175.816 |
| | 4 | −30.549 | −6.258 | 178.126 | | 6 | −13.771 | −9.037 | 170.827 |
| | | | | | | 7 | −9.290 | −7.679 | 172.799 |
| H-cap | 1 | −18.707 | 49.133 | 143.517 | | 8 | −8.945 | −7.971 | 171.168 |
| 108 atoms | 2 | −20.692 | −6.646 | 173.485 | | | | | |
| | 3 | −20.229 | −6.692 | 175.736 | | | | | |
| | 4 | −18.645 | −0.252 | 172.589 | H-cap | 1 | −17.362 | 46.889 | 142.440 |
| | 5 | −32.893 | −13.607 | 168.796 | 180 atoms | 2 | −12.926 | −7.625 | 170.714 |
| | | | | | | 3 | −8.869 | −6.359 | 173.275 |
| H-cap | 1 | −20.894 | 47.942 | 143.183 | | 4 | −8.973 | −7.237 | 170.824 |
| 126 atoms | 2 | −34.514 | −14.917 | 163.249 | | 5 | −9.193 | −5.344 | 170.698 |
| | 3 | −14.445 | −2.182 | 171.804 | | 6 | −7.621 | −5.613 | 171.483 |
| | 4 | −15.442 | −7.009 | 172.367 | | 7 | −10.231 | −8.320 | 172.018 |
| | 5 | −13.117 | −6.253 | 175.824 | | 8 | −12.137 | −2.022 | 171.460 |
| | 6 | −13.694 | −7.533 | 174.305 | | 9 | −30.190 | −14.732 | 162.479 |
| | | | | | | | | | |
| H-cap | 1 | −18.815 | 47.253 | 143.320 | | | | | |
| 144 atoms | 2 | −14.525 | −7.711 | 171.556 | | | | | |
| | 3 | −10.663 | −6.005 | 173.922 | | | | | |
| | 4 | −10.649 | −7.638 | 172.019 | | | | | |
| | 5 | −12.225 | −8.094 | 172.502 | | | | | |
| | 6 | −13.418 | −1.923 | 172.117 | | | | | |
| | 7 | −32.624 | −14.784 | 164.328 | | | | | |

[a] The atom numbers refer to the numbering scheme chosen in Figure 9.

As can be seen certain combinations of functionals and basis sets, such as VWN/DZP, offer fortuitous error compensation. For instance, using the more flexible TZP with the VWN functional instead results in a sizable change of the chemical shift of about 9 ppm away from the experimental value, which is to a large extent compensated when switching to the more accurate revPBE density functional. Compared to TZP, the TZ2P basis includes an additional set of 4f functions for each carbon and is thus prohibitively expensive for the larger systems studied here. The effect of the additional polarization functions on the carbon shift is not completely negligible but also not expected to be larger than additional correlation effects as well as self-interaction corrections that are not covered by the revPBE functional. The basis set and DFT trends obtained for $C_{60}$ are also found for the nanotube fragments that could be studied with the TZ2P basis; see Tables 2−5. Also, the trends obtained when using smaller basis sets than TZP are similar for $C_{60}$, the H-capped, and the $C_{30}$-capped tubes. Previous experience with NMR calculations shows that other nonhybrid gradient-corrected standard functionals do not offer significantly more accurate results in a systematic fashion. In summary, the revPBE/TZP level offers a reasonably accurate description of the systems covering the main effects from structure and electron correlation, with currently neglected correlation, self-interaction, basis set, vibrational and temperature, and intermolecular interaction effects adding up to acceptable deviations between theory and experiment estimated to be on the order of 5 ppm.

All computed chemical shifts for the nanotube fragments are listed in Figures 9 and 10 besides graphics of the SWNT fragments to allow for an easy comparison of the chemical shifts with the position of the respective carbon atom in the tube.

We note a number of trends: For the H-capped fragments, the chemical shifts at the ends are smaller than in the tube's center if the carbon is directly bound to a hydrogen; otherwise, it is larger. The values in the middle of the tube seem to approach a value of about 133 ppm from above for increasing length of the fragments. For the $C_{30}$-capped fragments, the shifts of carbons in the middle of a fragment are always smaller than at the end. The carbon shifts in the tips of the caps exceed the one for $C_{60}$ by about 14 ppm for the longest members. The carbon shifts in the middle of the fragments approach a value between 129 and 130 ppm, also from above. This chemical shift is in surprisingly good agreement with the experimental values of 126 and 124 ppm quoted above. It should be remembered that the experimental sample was certainly not consisting of only one type of tube. Nevertheless, the agreement is encouraging, in particular when considering, by comparison with our $C_{60}$ results, that the computed values are likely to overestimate experimental results by about 3 ppm.

The discrepancy between the central chemical shifts for the H-capped and the $C_{30}$-capped systems must be attributed to the different nature of the frontier orbitals. It cannot be expected that an orbital which is mainly localized at the tube's ends has a considerable direct contribution to the chemical shift of a carbon residing in the middle of a tube. However, from the preceding discussion it is obvious that there is a large effect of the HOMO on the energies of the HOMO-1 etc. which will have an influence on the $^{13}C$ chemical shifts (the expression for the paramagnetic shielding tensor contains $(\Delta E_{vo})^{-1}$, the inverse of the energy differences between virtual ($v$) and occupied ($o$) orbitals). As long as there is a noticeable interaction between the HOMO and the HOMO-1, say, with the latter yielding an important contribution to the shielding of one of the central carbons, the chemical shift is not converged. From our analysis of the frontier orbitals in the H-capped and the $C_{30}$-capped fragments, we believe that the chemical shifts of the latter are closer to the converged values for an infinite semiconducting (9,0) SWNT than the former. For longer

***Table 7.*** Principal Components of the Shielding Tensors $\sigma$ for the $C_{30}$-Capped (9,0) SWNT Fragments, Calculated at the TZP/revPBE Level

| system | no.[a] | $\sigma_{11}$ | $\sigma_{22}$ | $\sigma_{33}$ | system | no.[a] | $\sigma_{11}$ | $\sigma_{22}$ | $\sigma_{33}$ |
|---|---|---|---|---|---|---|---|---|---|
| $C_{30}$-cap | 1 | −54.855 | −20.547 | 169.399 | | 12 | −19.462 | −7.134 | 173.223 |
| 132 atoms | 2 | −73.399 | −0.788 | 171.485 | | 13 | −13.832 | 9.002 | 173.568 |
| | 3 | −13.618 | −9.476 | 171.543 | | 14 | −19.553 | 2.325 | 177.229 |
| | 4 | −17.825 | −5.531 | 174.944 | | 15 | −19.036 | −11.280 | 177.393 |
| | 5 | −16.680 | 1.469 | 179.943 | | 16 | −18.627 | 3.486 | 180.745 |
| | 6 | −13.085 | −3.738 | 170.601 | | 17 | −40.240 | −15.727 | 186.494 |
| | 7 | −48.568 | −3.745 | 171.960 | | 18 | −64.258 | −29.661 | 208.347 |
| | 8 | −48.570 | −18.930 | 178.213 | | | | | |
| | 9 | −51.820 | 19.884 | 159.685 | $C_{30}$-cap | 1 | −73.066 | −17.124 | 177.621 |
| | 10 | −17.923 | −3.517 | 173.797 | 186 atoms | 2 | −96.614 | −7.141 | 200.386 |
| | 11 | −10.121 | −4.780 | 174.218 | | 3 | −25.874 | −6.052 | 178.183 |
| | 12 | −21.016 | −0.573 | 179.455 | | 4 | −20.331 | −8.597 | 182.744 |
| | 13 | −28.048 | −15.425 | 176.717 | | 5 | −6.833 | −4.280 | 177.579 |
| | 14 | −42.689 | −28.806 | 183.416 | | 6 | −9.418 | −4.732 | 177.226 |
| | | | | | | 7 | −71.798 | −29.117 | 207.319 |
| $C_{30}$-cap | 1 | −63.216 | −18.600 | 173.169 | | 8 | −65.714 | −11.482 | 197.203 |
| 150 atoms | 2 | −72.678 | −16.578 | 185.763 | | 9 | −17.876 | −1.005 | 174.905 |
| | 3 | −18.683 | −16.252 | 182.339 | | 10 | −19.904 | 0.733 | 182.108 |
| | 4 | −19.226 | −3.985 | 174.222 | | 11 | −12.951 | −0.791 | 179.374 |
| | 5 | −8.204 | −6.767 | 180.216 | | 12 | −75.458 | −28.498 | 221.134 |
| | 6 | −53.602 | −28.239 | 195.313 | | 13 | −46.757 | −14.467 | 192.941 |
| | 7 | −33.637 | −14.688 | 182.012 | | 14 | −20.697 | 0.037 | 181.970 |
| | 8 | −21.776 | −2.541 | 180.317 | | 15 | −17.668 | −12.479 | 177.875 |
| | 9 | −13.536 | −12.552 | 179.037 | | 16 | −16.954 | −0.016 | 178.575 |
| | 10 | −55.645 | −31.505 | 195.389 | | 17 | −54.980 | 17.439 | 173.554 |
| | 11 | −52.994 | −11.019 | 182.348 | | 18 | −18.688 | −8.950 | 172.359 |
| | 12 | −16.291 | −0.831 | 172.776 | | 19 | −14.420 | 14.389 | 172.525 |
| | 13 | −18.489 | 0.746 | 180.770 | | 20 | −18.306 | −1.153 | 176.089 |
| | 14 | −54.870 | 21.436 | 162.962 | | | | | |
| | 15 | −17.792 | −4.290 | 171.203 | $C_{30}$-cap | 1 | −75.801 | −19.414 | 182.100 |
| | 16 | −15.776 | 8.056 | 173.419 | 204 atoms | 2 | −105.626 | −10.218 | 211.382 |
| | | | | | | 3 | −30.247 | −8.991 | 186.153 |
| $C_{30}$-cap | 1 | −65.426 | −20.424 | 175.059 | | 4 | −19.657 | −7.014 | 182.098 |
| 168 atoms | 2 | −88.549 | −6.774 | 191.149 | | 5 | −7.091 | −5.820 | 179.295 |
| | 3 | −21.624 | −9.277 | 177.436 | | 6 | −9.927 | −3.326 | 176.71 |
| | 4 | −16.061 | −5.150 | 176.648 | | 7 | −10.009 | 0.781 | 176.925 |
| | 5 | −11.231 | −5.494 | 178.138 | | | | | |
| | 6 | −6.959 | 3.786 | 176.016 | $C_{30}$-cap | 1 | −82.120 | −16.480 | 185.153 |
| | 7 | −15.480 | 3.244 | 179.219 | 222 atoms | 2 | −114.918 | −10.313 | 221.639 |
| | 8 | −9.917 | 1.730 | 169.453 | | 3 | −36.064 | −6.003 | 187.021 |
| | 9 | −59.091 | −7.026 | 186.617 | | 4 | −22.210 | −10.705 | 188.240 |
| | 10 | −65.415 | −21.775 | 194.876 | | 5 | −7.639 | −4.958 | 178.661 |
| | 11 | −53.849 | 20.352 | 167.893 | | 6 | −9.607 | −2.196 | 177.682 |
| | | | | | | 7 | −9.012 | −2.062 | 176.789 |

[a] The atom numbers refer to the numbering scheme chosen in Figure 10.

fragments, improved agreement with experimental estimates should be expected, in particular for the H-capped systems. This is due to the fact that for both systems the central carbon atoms should afford the same chemical shifts as the fragments approach infinite length.

To determine if the chemical shifts are dependent upon the symmetry of the $C_{30}$-capped SWNTs, a computation on the smallest tube possessing $D_3$ symmetry was made. Comparison of the results, shown in Figure 11, with the 132 atom tube of $D_{3d}$ symmetry shows that the shifts at the end of the tube are 3.45 and 6.11 ppm larger for the former than for the latter. Moreover, for the $D_3$ tube, shifts in the middle range from ∼124−136 ppm, whereas, for the $D_{3d}$ tube, the shifts near the middle are 131.99 and 130.19 ppm. Under the assumption that the shifts are converged for the 132 atom $D_3$ member, we can conclude that the $D_3$ set will have a larger chemical shift range than the $D_{3h}/D_{3d}$ series; however, the average of this range will not be significantly different than the shift predicted for the energetically more stable species. The 132 atom $D_3$ tube is predicted to be 4.85 kcal/mol less stable than the $D_{3d}$ tube in our calculations. This is in agreement with other DFT calculations.[12]

For completeness, we also report the calculated principal components of the shielding tensors. From the data collected in Tables 6 and 7, it can be seen that the shielding tensor components converge in a way similar to that of the chemical shifts when increasing the tube length albeit not as smoothly as the isotropic shieldings. The shielding tensors are strongly anisotropic. For $C_{60}$, the shielding tensor affords a large positive component perpendicular to the "buckyball's" surface, and two negative component within the surface that are an order of magnitude smaller (Figure 12). The shielding tensors for the H-capped and $C_{30}$-capped SWNTs are very similar in the tube's center. These, as well as the shielding tensors at the tip of the caps in the $C_{30}$-capped systems, are qualitatively comparable to $C_{60}$ in the sense that the large diamagnetic component is perpendicular to the carbon framework. Generally, in the middle of the tube fragments, the negative components within the surface are significantly smaller in magnitude than for $C_{60}$. The smaller chemical shift for the (9,0) SWNT compared to $C_{60}$ is seen to result both from an increase of the magnitude of the positive $\sigma_{33}$ component and a decrease of the magnitude of the negative $\sigma_{11}$ and $\sigma_{22}$ components.

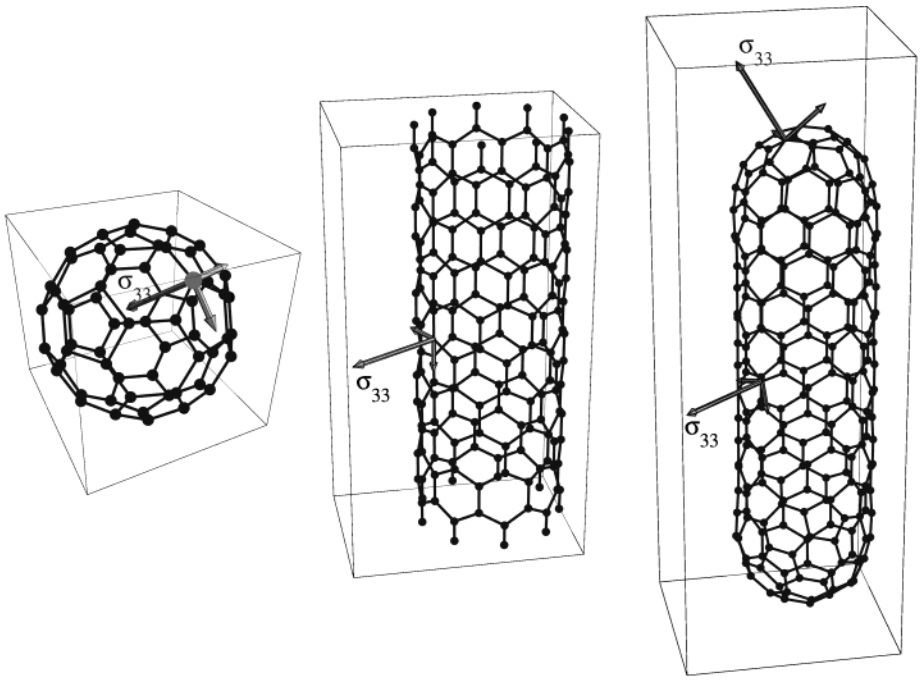


***Figure 12.*** Orientation of the calculated shielding tensors for $C_{60}$ and the largest H- and $C_{30}$-capped nanotube fragments. The arrows indicate the principal axes. The arrows' lengths reflect the magnitude of the principal shielding components. For reasons of clarity of presentation, they are not exactly proportional. The large diamagnetic $\sigma_{33}$ component is indicated. See Tables 6 and 7 for numerical data (180-atom H-capped tube: atom no. 5. 222-atom $C_{30}$-capped tube: atoms no. 1 and 7). See Figures 9 and 10 for numbering.

## 4. Summary and Conclusions

In this work we have, to the best of our knowledge, presented the first density-functional study of NMR chemical shifts in single-wall carbon nanotube (SWNT) fragments. The study was carried out for the nonhelical (9,0) system. In agreement with recent computational and experimental studies, the (9,0) SWNT is predicted to have a finite band gap around the Fermi level. The analysis of the energies and the nature of the frontier orbitals indicates that hydrogen capped tube fragments are not necessarily good models of the infinite systems, at least not at sizes which are currently accessible to first-principles molecular calculations. The HOMO and LUMO themselves need to be considered as artifacts when making attempts to compare with the infinite systems. In contrast, the $C_{30}$-capped SWNT fragments appear to represent good models for the infinite systems. Their properties converge reasonably fast with increasing length of the fragments. The chemical shift for the (9,0) SWNT is estimated from our calculations to be around 130 ppm which is in encouraging agreement with experimental estimates. Comparison between a tube of $D_{3d}$ and one of $D_3$ symmetry indicates that tubes in the latter set may have a broader chemical shift range, whose average lies near the value predicted for the $D_{3d}/D_{3h}$ series. A more comprehensive study which will further address the influence of the tube diameter on the chemical shifts is in progress. When taking the theoretical predictions by Latil et al.[19] for the difference between semiconducting and metallic SWNTs into consideration (metallic systems were found to be 11 ppm less shielded), and assuming that the result for the (9,0) tube is typical for a semiconducting system, metallic tubes' chemical shifts can be expected to be close to the one for $C_{60}$.

**Acknowledgment.** J.A. acknowledges support from the Center of Computational Research at the University of Buffalo, SUNY. E.Z. acknowledges financial support from the "International Max-Planck Research School for Advanced Materials" (IMPRS-AM) as well as informative discussions with Jiri Cech regarding experimental aspects of nanotube synthesis and characterization. We further acknowledge help from Dr. Boris Le Guennic regarding the figures. We thank Dr. Siegmar Roth for valuable comments on the manuscript.

JA047941M